Review of Scientific Instruments

RESEARCH ARTICLE | JULY 01 2022

# PIONEER, a high-resolution single-crystal polarized neutron diffractometer

**Special Collection:** New Science Opportunities at the Spallation Neutron Source Second Target Station

Yaohua Liu ; Huibo Cao ; Stephan Rosenkranz ; Matthew Frost ; Thomas Huegle ; Jiao Y. Y. Lin ; Peter Torres ; Alexandru Stoica; Bryan C. Chakoumakos



*Rev. Sci. Instrum.* 93, 073901 (2022)
https://doi.org/10.1063/5.0089524

Review of Scientific Instruments ARTICLE scitation.org/journal/rsi

# PIONEER, a high-resolution single-crystal polarized neutron diffractometer

Cite as: Rev. Sci. Instrum. 93, 073901 (2022); doi: 10.1063/5.0089524
Submitted: 26 February 2022 • Accepted: 8 June 2022 •
Published Online: 1 July 2022



Yaohua Liu,[1,a)] Huibo Cao,[2] Stephan Rosenkranz,[3] Matthew Frost,[4] Thomas Huegle,[4] Jiao Y. Y. Lin,[1] Peter Torres,[1] Alexandru Stoica,[2] and Bryan C. Chakoumakos[2]

## AFFILIATIONS

[1] Second Target Station, Oak Ridge National Laboratory, Oak Ridge, Tennessee 37831, USA
[2] Neutron Scattering Division, Oak Ridge National Laboratory, Oak Ridge, Tennessee 37831, USA
[3] Materials Science Division, Argonne National Laboratory, Lemont, Illinois 60439, USA
[4] Neutron Technology Division, Oak Ridge National Laboratory, Oak Ridge, Tennessee 37831, USA

**Note:** Paper published as part of the Special Topic on New Science Opportunities at the Spallation Neutron Source Second Target Station.
[a)] **Author to whom correspondence should be addressed:** liuyh@ornl.gov

## ABSTRACT

PIONEER is a high Q-resolution, single-crystal, polarized neutron diffractometer at the Second Target Station (STS), Oak Ridge National Laboratory. It will provide the unprecedented capability of measuring tiny crystals (0.001 $mm^3$, i.e., x-ray diffraction size), ultra-thin films (10 nm thickness), and weak structural and magnetic transitions. PIONEER benefits from the increased peak brightness of STS cold-neutron sources and uses advanced Montel mirrors that are able to deliver a focused beam with a high brilliance transfer, a homogeneous profile, and a low background. Monte Carlo simulations suggest that the optimized instrument has a high theoretical peak brilliance of $2.9 \times 10^{12}$ n $cm^{-2}$ $sr^{-1}$ $Å^{-1}$ $s^{-1}$ at 2.5 Å at the sample position, within a $5 \times 5$ $mm^2$ region and a $\pm 0.3^\circ$ divergence range. The moderator-to-sample distance is 60 m, providing a nominal wavelength band of 4.3 Å with a wavelength resolution better than 0.2% in the wavelength range of 1.0–6.0 Å. PIONEER is capable of characterizing large-scale periodic structures up to 200 Å. With a sample-to-detector distance of 0.8 m, PIONEER accommodates various sample environments, including low/high temperature, high pressure, and high magnetic/electric field. A large cylindrical detector array (4.0 sr) with a radial collimator is planned to suppress the background scattering from sample environments. Bottom detector banks provide an additional 0.4 sr coverage or can be removed if needed to accommodate special sample environments. We present virtual experimental results to demonstrate the scientific performance of PIONEER in measuring tiny samples.



## I. INTRODUCTION

Neutron scattering has played seminal roles in our understanding of advanced materials, revealing the microscopic details on the interplay among spin, charge, orbital, and lattice degrees of freedom and their collective excitations. As formulated in the Basic Energy Sciences Advisory Committee (BESAC) report *Challenges at the Frontiers of Matter and Energy: Transformative Opportunities for Discovery Science*[1] and the *Basic Research Needs Report Quantum Materials for Energy Relevant Technology*,[2] the contemporary scientific grand challenges need basic research on "quantum materials," "critical roles of heterogeneity, interfaces, and disorder," and "beyond-equilibrium matter," which requires sophisticated instruments to probe the structure and dynamics of materials over extended length, time, and energy scales. To address this need, Oak Ridge National Laboratory (ORNL) is substantially expanding the capabilities of the Spallation Neutron Source (SNS) to build the Second Target Station (STS) with a high-brightness cold-neutron source, i.e., a source optimized for long-wavelength neutrons. The high peak brightness of cold neutrons and the broad wavelength band available at the STS will lead to transformative capabilities, such as studying smaller samples, performing time-resolved studies, and investigating hierarchical architectures in detail.[3] The new STS instruments will utilize the latest advances in neutron optics, neutron spin manipulation, instrument design, and computational techniques, which will enable researchers to

collect information faster and with higher precision than existing instruments.

PIONEER at the STS will be a next-generation time-of-flight (TOF) single-crystal diffractometer for materials science, which aims at accelerating materials discovery with the world-leading capability to investigate samples with tiny volumes or weak signals in a range of experimental conditions. Single-crystal neutron diffraction (SCND) is a powerful structural characterization tool for materials science, including quantum magnets, superconductors, energy and functional materials, and minerals. Particularly, SCND provides critical and accurate microstructural information about hydrogen-related energy materials and exotic magnetic materials due to its high sensitivity to the arrangement of light elements and magnetic moments. However, neutron scattering is generally a flux-limited technique, and SCND has known constraints. For SCND, the required sample size is traditionally larger than 1 $mm^3$, and the beamtime capacity and sample environments (SEs) need expansion to match the demand from the user community. The sample-size barrier is gradually overcome by developing higher brightness moderated neutron sources and detectors of greater sensitivity. Particularly, accelerator-driven spallation neutron sources have enabled highly efficient SCND instruments using the TOF Laue technique and large-area detectors. SCD at the Intense Pulsed Neutron Source (IPNS)[4] and SXD at the ISIS Neutron and Muon Source[5] are two early successful examples. Recently built instruments include TOPAZ at ORNL[6] and SENJU at the Japan Proton Accelerator Research Complex (J-PARC),[7] both of which use a MW-class proton accelerator and an extensive detector array. These instruments have greatly reduced the required sample volume to below ~0.1 $mm^3$, but it is still larger than the typical x-ray diffraction size. Currently, MAGiC, a permanently polarized instrument, is under construction at the European Spallation Source (ESS),[8,9] aiming to push the crystal-size requirement to 0.001 $mm^3$ and focusing on magnetism-related studies. PIONEER will also enable measurements on 0.001 $mm^3$ or smaller samples but plan to support broader fields in materials science.

This paper gives an overview of the proposed science cases for PIONEER, describes its technical parameters and major instrument components, and presents detailed Monte Carlo ray-tracing simulation results to demonstrate its performance. PIONEER is currently under the active preliminary design, and the instrument parameters are subject to change.

## II. SCIENCE CASES AND INSTRUMENT SPECIFICATIONS

PIONEER aims to provide the world-leading single-crystal neutron diffraction capabilities to measure tiny crystals (0.001 $mm^3$, i.e., x-ray diffraction size) and ultra-thin films (10 nm thickness) and weak structural and magnetic transitions. With the input from the user community, the science advisory team has identified a broad range of research areas that can benefit from unprecedented capabilities of PIONEER. For example, PIONEER requires a small sample volume that is one-order-of magnitude smaller than the current limit. It assists materials discovery at the early stage before large single crystals are available. It enables studies of rare and valuable natural mineral inclusions (usually less than 500 $\mu$m) in diamond. At the same time, PIONEER can probe exotic magnetic states in thin films and even surface and interface states. It also enables studies of high-pressure induced quantum states using commercially available x-ray diamond avail cells. PIONEER has a high reciprocal-space resolution to probe chemically and magnetically modulated structures with a large characteristic length scale up to 200 Å and to study large unit-cell functional materials, such as metal–organic frameworks and polyoxometalates. The instrument provides a high-flux polarized neutron beam that can significantly enhance the sensitivity of the local magnetic susceptibility.[10–13] The high brightness, the broad wavelength band, and the large detector array lead to high efficiency for time-resolved studies and few-pulse experiments. This also allows measuring both Bragg reflections and diffuse scattering simultaneously from sub-$mm^3$ crystals that help researchers to decipher both the average and local structures in crystalline samples. Furthermore, PIONEER supports various sample environments for materials science, including low/high temperatures, magnetic/electric fields, and pressure.

**TABLE I.** Instrument parameters for PIONEER. The brilliance is evaluated at the sample position over a square region of 5 mm wide with a ±0.3° divergence for both horizontal and vertical directions, which is in the unit of n $cm^{-2}$ $sr^{-1}$ $Å^{-1}$ $s^{-1}$. The simulations are performed on an ideal beamline. See the main text for details.

| Parameter | Value | Comment |
|---|---|---|
| Moderator | Pure parahydrogen | Cylindrical, port 13 |
| $\lambda$ range | 1.0–6.0 Å | |
| $\lambda$ bandwidth | 4.0 Å | Nominal 4.3 Å |
| $\delta Q/Q$ | <0.3% | Minimum value |
| $L1$ | | Moderator to sample |
| Fixed | 60.0 m | |
| $L2$ | | Sample to detector |
| Standard | 0.8 m | |
| Maximum | 1.2 m | |
| Detector coverage | | With collimators |
| Side cylindrical | 4.0 sr | |
| Bottom flat | 0.4 sr | |
| Beam divergence | | |
| Maximum | ±0.3° | Standard mode |
| Minimum | ±0.1° | High resolution mode |
| Beam size | | Tunable |
| Maximum | 5 × 5 $mm^2$ | |
| Minimum | 0.5 × 0.5 $mm^2$ | |
| Q coverage | | |
| Unpolarized beam | 0.1–12.0 $Å^{-1}$ | |
| Polarized beam | 0.1–8.0 $Å^{-1}$ | |
| Brilliance | | 15 pulses per second |
| 5 × 5 $mm^2$, ±0.3° | 2.9 ×$10^{12}$ | Peak value at 2.5 Å |
| Flux | | 4 Å band |
| 1 × 1 $mm^2$, ±0.3° | 6.8 × $10^8$ n $cm^{-2}$ $s^{-1}$ | 1.5–5.5 Å |

Overall, PIONEER will expand the frontier of SCND, particularly in the following areas:[1–3,14] (1) quantum materials, such as unconventional superconductivity, 4d–5d strong spin-orbital coupling systems, and topological materials; (2) thin films and artificial heterostructures; (3) functional materials for energy, such as metal–organic frameworks, polyoxometalates, multiferroic oxides, complex hybrids, and thermoelectric materials; (4) time-resolved studies, and (5) planetary sciences and mineral physics.

To maximize the scientific performance of PIONEER, we consider the following principles for the instrument design: (1) PIONEER shall transport a high-brilliance beam to the sample position, remove undesired neutrons from the incident beam as early as possible, have a large detector array, and minimize neutrons not directly scattered by samples from reaching the detector. (2) The end station shall accommodate the most common types of sample environments (SEs) used at the leading neutron facilities for materials science and be flexible for user-provided SEs and future upgrades. (3) The instrument system shall provide a homogeneous beam at the sample position and precise control on the sample position to enable high-quality data collection for quantitative structural analysis. (4) It shall enable remote operation for most experiments, if not all, and enable autonomous experiments as many as reasonably achievable. After balancing the requirement from the proposed science cases and the technical constraints, we have chosen the specifications for the PIONEER, as listed Table I. The standard beam divergences are similar at TOPAZ, SENJU, MAGiC, and PIONEER instruments, but the sample size requirements are different for the four instruments. The former is mainly determined by crystal mosaicity, while the latter is primarily affected by individual instrument characteristics. In Sec. III, we describe the major components of the instrument and present the simulated performance.

## III. INSTRUMENT SYSTEM

Figure 1 shows a schematic of the PIONEER instrument. PIONEER will use beam port 13 to extract the beam from the upper pure-parahydrogen moderator, which is a vertical cylinder and provides a narrower neutron pulse width for a better wavelength resolution than the bottom tube moderator.[3] Figure 2 shows the wavelength resolution $\delta\lambda/\lambda$ for different moderator-to-sample distances $L1$. The calculation uses the moderator source file simulated for beam port 13 [*BL13-CY-46D-STS-Min-2G-source_mctal-125_sp.dat* (2021)]. We have chosen $L1 = 60$ m, and as seen from Fig. 2, at this distance, this instrument provides $\delta\lambda/\lambda$ below or near 0.2% over the wavelength range of 1.0–6.0 Å.

As previously mentioned, the transport system shall efficiently transport neutrons from the source to the sample position with an illumination area of $5 \times 5$ mm$^2$ with a $\pm 0.3^\circ$ beam divergence in both the horizontal and vertical directions. The angular and spatial distribution of the neutron flux shall be homogeneous within this phase space, and the neutron flux should quickly vanish outside this phase space. From the moderator, the first optical component is the beam extraction system acting as a collimator, which starts before the monolith[3] and ends before the primary mirror. The collimator is interrupted by the maintenance shutter located right outside the monolith at 5.75 m. Inside the bunker wall, two bandwidth choppers select the wavelength band. The neutron transport vacuum system begins after the maintenance shutter to minimize air scattering. The operational shutter is outside of the bunker wall at 13.9 m, used for daily operations, such as sample or sample environment changes.

We choose a pair of Montel Kirkpatrick–Baez (KB) mirrors (also known as nested KB mirrors) for the beam transport because



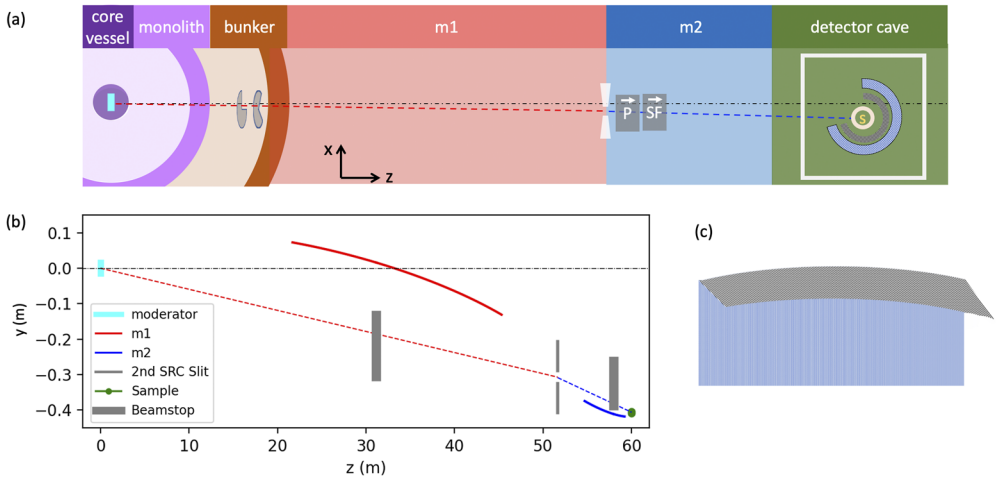


**FIG. 1.** (a) (Top view) Schematic drawing of the PIONEER layout to show the key regions, including the monolith, the bunker, the primary mirror (m1) and secondary mirror (m2) regions, and the detector cave. The red and blue dashed lines indicate the major axes of the Montel mirrors m1 and m2, respectively. The black dot-dashed line is a guide to the eye to show the rotations of the major axes. The shown components are the moderator, a pair of wavelength band choppers, the secondary source slit, the removable polarizer, and spin flipper, and the detector. The gray and light-blue arcs inside the detector cave represent the oscillating radial collimator and the detector bank. (b) (Side view) The major beam transport components are a pair of Montel mirrors with built-in beam stops and one set of slits at the secondary source position. m1 and m2 are 21.0 and 4.0 m long, respectively. Two additional sets of slits are placed right before m1 and right after m2 (not shown). The three sets of slits are used to control the beam size and divergence at the sample position. (c) A sketch of a Montel mirror consisting of two elliptical reflection surfaces that are mutually perpendicular.

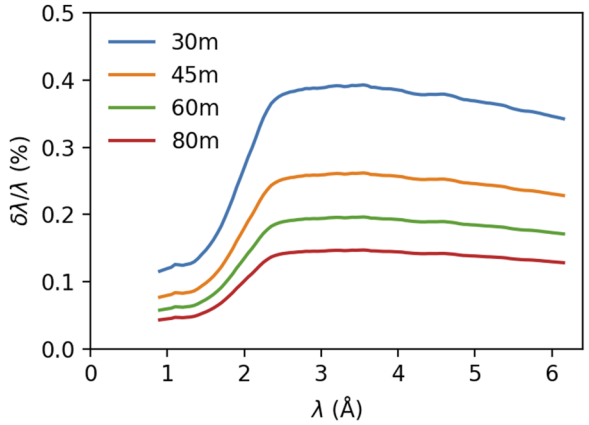


**FIG. 2.** Wavelength resolution as a function of the moderator-to-sample distance $L1$. PIONEER chooses $L1$ = 60 m to achieve $\delta\lambda/\lambda$ below or near 0.2% over 1.0–6.0 Å.

they provide excellent focusing with a high brilliance transfer (BT) and high beam homogeneity at the sample position.[15–17] As sketched in Fig. 1, each Montel mirror has two elliptical reflection surfaces arranged perpendicularly to each other. The mirror parameters are optimized using McStas[18] and SciPy[19] packages taking the gravity effect into account. The mirror specifications are listed in Table II. The primary Montel mirror (m1) starts from 21.7 m and ends at 41.7 m. m1 is looking at the moderator with its major axis being titled both right and down by 0.34°. The major axis of m1 runs in a straight line to the secondary source location. A beamstop at the mid-distance of m1 blocks the downstream optics from the line-of-sight to the moderator. m1 will generate a focused beam and generate the secondary source at 51.66 m. Between the secondary source and the secondary Montel mirror (m2), a removable polarizing V-cavity and an adiabatic spin-flipper will generate a polarized neutron beam when needed. m2 is looking at the secondary source and is 4.0 m long. The major axis of m2 is further tilted right and down by 0.34° to form a kinked beamline geometry.

Multiple slits along the beamline will control the beam size and divergence. The most important three are at 21.50 m (before m1), 51.65 m (at the secondary source location), and 59.2 m (after the secondary mirror). The polarization system will provide an effective polarized beam with $\lambda_{cutoff} \leq 1.5$ Å and $Q_{max} \geq 8$ Å, and a magnetic guide field in the order of 1 mT will be used afterward to maintain the direction of the spin and polarization of the neutron beam. The tilted and kinked beamline geometry can keep the average beam in the truly horizontal plane at the sample position and move the sample out of the line-of-sight of the moderator, as illustrated in Fig. 1.

**TABLE II.** Technical parameters for the Montel mirrors used at PIONEER.

| Parameter | Primary mirror, m1 | Secondary mirror, m2 |
|---|---|---|
| Length (m) | 21.0 | 4.0 |
| Start (m) | 21.70 | 54.75 |
| Major axis (m) | 51.66 | 8.34 |
| Minor axis (m) | 0.40 | 0.066 |
| Rotation (deg) | | |
| Right | 0.34° | 0.68° |
| Down | 0.34° | 0.68° |

## A. Neutron transportation performance

The Elliptic_guide_gravity component from the McStas package[18] is used to model the Montel mirrors. To benchmark the optimal performance, we have used the mirror coatings[20] of $m = 6$ for two mutually perpendicular surfaces and $m = 0$ for the other two surfaces and used the slope value of $\alpha = 3.044$ Å. The parameter $\alpha$ is used to describe one major imperfection from realistic supermirrors. Neutrons reflected with a high wavelength transfer are not totally reflected by a supermirror, and the reflectivity drops rapidly at the extended critical scattering vector of a supermirror, $q_c = m \times q_c^{Ni}$, where $q_c^{Ni} = 0.021\,9$ Å$^{-1}$ is the critical scattering vector for Ni. A linear function is used to model the reflection probability in the intermediate $q$ values, i.e., $R(q) = R_0(1 - \alpha(q - q_c^{Ni}))$ for $q_c > q > q_c^{Ni}$, where $R_0$ is the reflectivity below $q_c^{Ni}$. Other coating parameters take the default values. An in-depth analysis of the position-dependent coating requirement is in progress. To evaluate the mirror performance over a wavelength band broader than 4 Å, choppers are not included in the simulations.

Figure 3 shows the simulated brilliance transfer (BT)[21] and the absolute brilliance at the sample position. The BT is a metric to

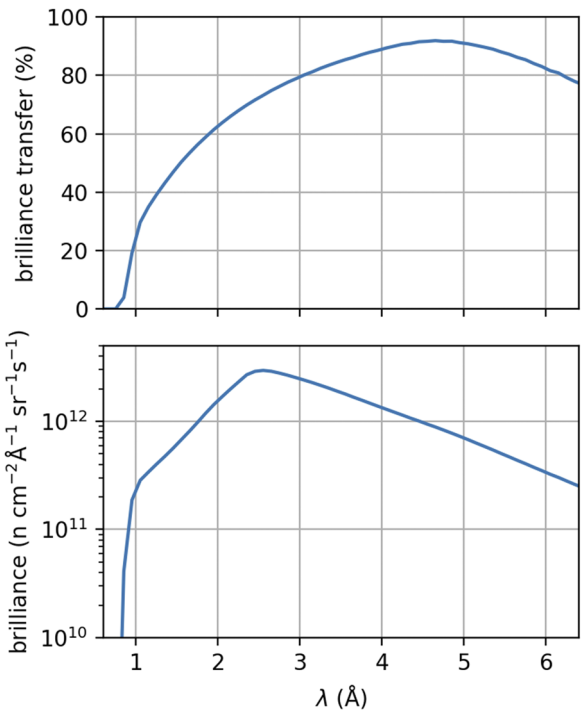


**FIG. 3.** (a) Brilliance transfer and (b) absolute brilliance at the sample position evaluated over a 5 mm wide square region and a ±0.3° divergence range in both the horizontal and vertical directions.

quantify the performance of the optical system to transport neutrons from the source to the sample and has a theoretical maximal value of 100% according to Liouville's theorem.[21] The brilliance is evaluated over a 5 × 5 mm$^2$ region of interest (ROI) and a ±0.3° range in both the horizontal ($x$) and vertical ($y$) directions. The angular and spatial ROIs are also shown in Figs. 4 and 5, respectively. Within 1.0–6.0 Å, the BT initially increases as $\lambda$ increases, becomes more than 60% at $\lambda$ = 2.0 Å, and peaks around 4.7 Å with a value exceeding 90%. The decrease in the BT at longer wavelengths is due to the gravity effect. The peak value of the absolute brilliance is 2.9 × 10$^{12}$ n cm$^{-2}$ sr$^{-1}$ Å$^{-1}$ s$^{-1}$ at 2.5 Å (also listed in Table I), which is largely determined using the STS source characteristics.[3] The simulation assumes an ideal instrument and has not taken misalignment or waviness of the mirrors into account, which are known to deteriorate the performance,[22,23] particularly for long beamlines. Effects of such realistic imperfections are under investigation, and our preliminary analysis suggests that they may cause a flux reduction in the order of 20%, and details will be reported elsewhere.

The beam homogeneity at the sample position is shown in Figs. 4 and 5. Figure 4 presents the angular distribution of the neutron flux averaged over the 5 × 5 mm$^2$ ROI. The results from a 4 Å band of 1.5–5.5 Å and a 0.4 Å band centered at 2.5 Å are shown in Figs. 4(a) and 4(b), respectively. Figures 4(c) and 4(d) show linecuts along the horizontal direction. The results are similar for the vertical and horizontal directions, except at the long-wavelength end, where the gravity effect slightly skews the beam direction in the vertical direction (data not shown). These simulations confirm that the optimized transport system gives rise to a homogeneous angular distribution. The flux-weighted average beam direction in the 1.5–5.5 Å band is within 0.002° from the absolute horizontal plane, indicating a truly horizontal neutron beam.

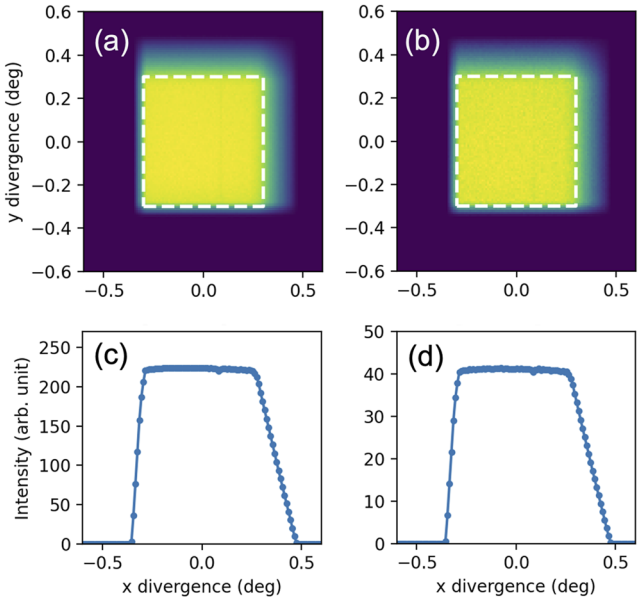


**FIG. 4.** Angular distribution of the neutron flux at the sample position. The neutron flux is integrated over a 5 × 5 mm$^2$ region within (a) 1.5–5.5 Å and (b) 2.3–2.7 Å. The dashed lines indicate the region of interest from the beam divergence requirement. (c) and (d) Flux distribution as a function of the beam direction in the horizontal plane (the $x$ direction), where the flux is integrated along the $y$ directions from (a) and (b), respectively.

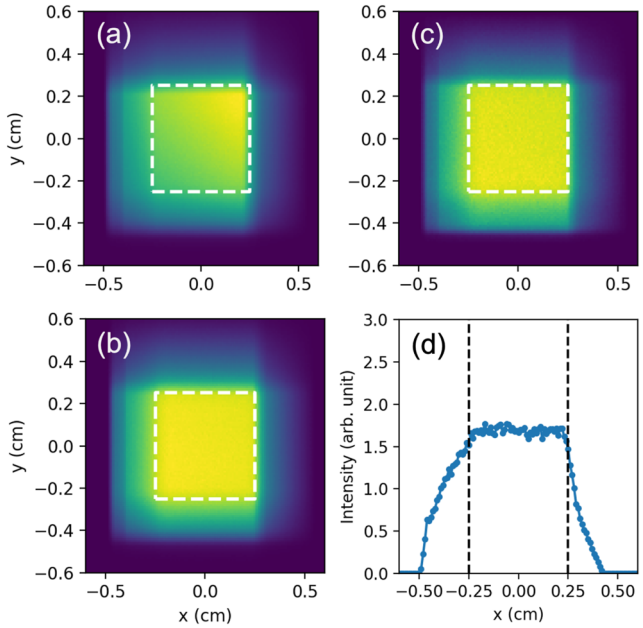


**FIG. 5.** Spatial distribution of the neutron flux at the sample position. The neutron flux is integrated over 1.5–5.5 Å (a) with all beam directions and (b) within the ±0.3° range. (c) The neutron flux is integrated over 2.3–2.7 Å within the ±0.3° range. (d) One-dimensional cut of (c) of the central 0.2 cm (i.e., $y$ = [−0.1, 0.1] cm) region. The dashed lines are the boundary of the 5 × 5 mm$^2$ square ROI.

Figures 5(a) and 5(b) plot the spatial distribution of the neutron flux over the 1.5–5.5 Å band. Neutrons of all directions are taken into account in Fig. 5(a), while only the neutrons within the ±0.3° range are included in Fig. 5(b). Although the beam is homogeneous within the required spatial and angular ROIs, the flux outside the ±0.3° range leads to beam inhomogeneity within the 5 × 5 mm$^2$ ROI and undesired neutrons outside this spatial ROI. As mentioned earlier, slits at various locations will fine-tune the beam divergence and footprint at the sample position.

Figures 5(c) and 5(d) indicate that the beam profile within the ±0.3° range is homogeneous within the 5 × 5 mm$^2$ ROI using the 2.3–2.7 Å band as an example. Coupled with the angular distribution, the spatial distribution weakly depends on the neutron wavelength. The beam profile is of high homogeneity in the central region of the 1.0–6.0 Å range. However, at both ends of this range, the beam is less homogeneous because the short- and long-wavelength neutrons are subjected more to the effects from the reflectivity slope below the critical edge and the gravity, respectively.

## B. End station

Figure 6 shows the detector system of PIONEER, which contains a vertical cylindrical array and a bottom flat array using silicon-photomultiplier (SiPM) based neutron Anger cameras.[3,24]

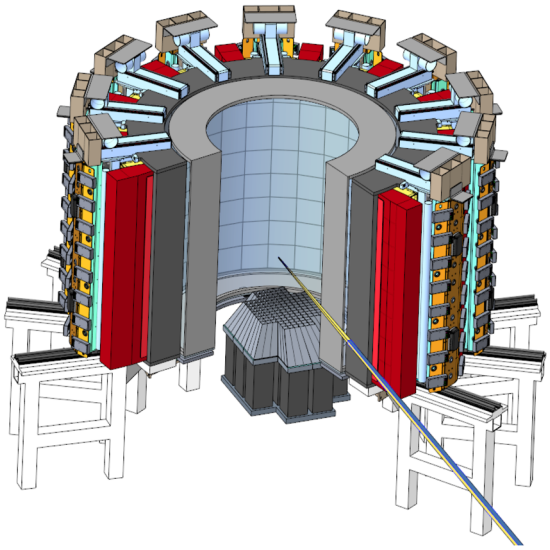

**FIG. 6.** PIONEER detector system contains a vertical cylindrical array with an oscillating radial collimator and a removable bottom flat array with a cone collimator. The radial collimator is omitted for clarity. The last portion of the neutron flight tube is included to indicate the direct beam direction.

The Anger camera principle is based on sharing of scintillation light among clusters of pixel sensors. A transparent light-spreading layer is placed between the scintillator and the sensor. The signals from several adjacent pixels are combined to produce an order of magnitude higher position resolution than the pixel pitch. For a typical Anger camera, the position resolution is about 10% of the pixel pitch size. Recent developments on the SiPM-based readout with a 7.2 mm pixel pitch show a position resolution better than 0.5 mm and high tolerance to magnetic stray fields, which are the preferred choice for PIONEER. The vertical and bottom arrays have 159 and 16 modules, respectively. Each module has a flat neutron active area of 172.6 × 172.6 $mm^2$, consisting of 3 × 3 SiPM units. There is a ~8-mm neutron insensitive region between adjacent modules. Using new-generation SiPM-based Anger cameras with a smaller pixel pitch and a higher counting rate is currently under evaluation.

The vertical cylindrical and bottom flat detectors will be equipped with an oscillating radial collimator[25] and a 3D-printed cone collimator,[26] respectively. The cylindrical detector has a sample-to-detector distance of 0.8 m, accommodating numerous types of sample environments (SEs) for materials science with the collimator in place. The cylindrical detector covers a solid angle of 4.0 sr, with 245° horizontal and 80° vertical ranges, and the bottom detector coverage is 0.4 sr.

The radial collimator for the cylindrical detector is removable to accommodate very large SEs. When needed, the sample-to-detector distance of the cylindrical detector can be increased to 1.2 m by moving detector modules away. However, there will be large gaps between detector modules and the solid-state coverage will be less in this case. The bottom detector array can be removed for extra-large SEs. To use an automatic sample changer, the bottom detector will be replaced with a goniometer; a cyrostream system[27] will provide the temperature control between 90 and 450 K, and a six-arm robotic arm[28] will be deployed for sample changes.

### C. Sample environments

The planned SEs are listed in Table III, most of which are currently available to users at the First Target Station (FTS) at the SNS.[31] Due to the instrument characteristics, PIONEER will excel when using extreme sample environments, particularly for the high-pressure and pulsed-magnetic-field experiments.

The tiny-sample capability offers advantages to use diamond anvil cells (DACs) for neutron scattering, which is under active development at ORNL.[30] For powder samples, the highest pressure achieved at the SNAP instrument is 120 GPa. However, the highest pressure is only around 20 GPa to date for single-crystal diffraction due to the inherent limitation of single-crystal samples. With smaller volumes, single-crystal samples tend to have a higher quality and thus a better chance to survive at high pressure. PIONEER provides a tunable beam size that can match the sample size and reduce the background scattering from the cell. Furthermore, the unprecedented capability of PIONEER to measure tiny crystals down to 0.001 $mm^3$ or less also opens the door to use the commercially available x-ray DACs for neutron diffraction experiments.

One of the critical technical issues for pulsed-magnetic-field experiments is that the field apparatus may fail before a sufficient signal/noise is achieved. PIONEER will collect valuable datasets with fewer pulses and increase the success rate with high peak brightness and low background.

### D. Performance evaluation

The target of measuring 0.001 $mm^3$ crystals at PIONEER is about 50 times smaller than the current limit at TOPAZ (~0.05 $mm^3$).[27] The small beam option, a long beamline, and a large sample to detector distance provide new opportunities for PIONEER to reduce the background level for measuring tiny crystals. PIONEER will provide sub-mm beam options, much smaller

**TABLE III.** Planned sample environment sets for PIONEER. Ultra-low T inserts include both $^3$He and dilution refrigerator inserts.

| Parameter | Value | Comments |
|---|---|---|
| Temperature | | |
| Standard | 1.5–500 K | Closed cycle refrigerator |
| Ultra-low T inserts | 0.05–300 K | |
| Cyrostream | 90–450 K | |
| Furnace | 300–1700 K | |
| Magnetic field | | |
| Static, max. | 14 T | 0.1–300 K, vertical |
| Pulsed, max. | >40 T | 1.5–300 K, horizontal[29] |
| Pressure | | |
| Clamp cell, max. | 2 GPa | 0.3–300 K |
| DAC, max. | >45 GPa | 0.3–300 K[30] |

than the smallest one at TOPAZ (2 mm diameter). To further minimize the background level at PIONEER, we have chosen to install the bandwidth choppers inside the bunker, avoid a direct line of sight between the moderator and the sample, employ scattering beam collimators, and use a vacuum sample vessel.

As listed in Table I, the integrated flux is $6.8 \times 10^8$ n cm$^{-2}$ s$^{-1}$ for the high-flux mode at 0.7 MW, which is about 14 times higher than that of TOPAZ ($4.7 \times 10^7$ n ·cm$^{-2}$ s$^{-1}$ at 1.4 MW). At the same time, PIONEER mainly uses neutrons from 1 to 6 Å (medium, 3.5 Å) for a relatively lower $Q$ range than TOPAZ, which mainly uses 0.4–3.5 Å neutrons (medium, 1.95 Å). Therefore, PIONEER will have an additional 3.2 gain factor on the scattering signal because the effective flux $\phi_{eff}(\lambda) = \phi(\lambda) \times \lambda^2$, where $\phi(\lambda)$ is the wavelength-dependent flux. The detector of PIONEER will have a solid angle coverage of 4.4 sr, about 1.4 times more than the current coverage of TOPAZ (3.2 sr, TOPAZ has 25 of 48 detector ports populated with Anger camera modules so far). Therefore, PIONEER will have about 60 times higher data collection rate than the current TOPAZ.

## IV. VIRTUAL EXPERIMENTS

This section presents a couple of virtual experiments to demonstrate the capability of PIONEER to measure tiny sample volumes and collect useful data with a few neutron pulses. The simulations use the MCViNE package.[32,33] Instrument background scattering has not been included in these simulations. However, the simulations have helped us determine the background level required to measure 0.001 mm$^3$ or smaller crystals at PIONEER.

In the first case, we have simulated experiments on a triangular lattice magnet $CsV(MoO_4)_2$[34] using a 0.125 mm$^3$ crystal (a cubic of 0.5 mm per side) and the wavelength band of 1–5 Å. Since PIONEER is a TOF Laue diffractometer with an extensive detector array, it probes a large reciprocal-space volume even at a fixed sample orientation. Figure 7(a) shows a two-dimensional slice in the volumetric reciprocal space covered from a single sample orientation. Figure 7(c) reports the number of peaks as a function of measuring time at this orientation after scaling down the intensity by the sample volume to 0.001 mm$^3$. It suggests that in the ideal case, one can observe more than 30 peaks with a signal-to-noise

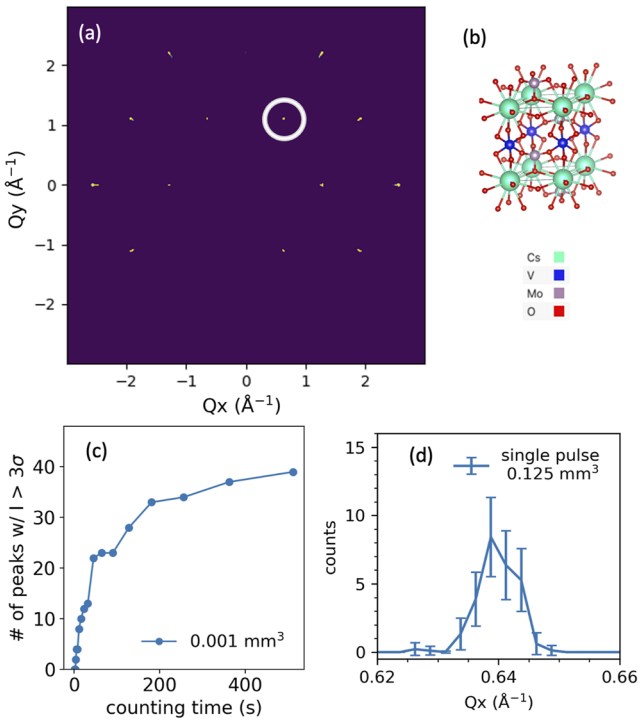


**FIG. 7.** Virtual experimental results from $CsV(MoO_4)_2$. (a) A slice in the reciprocal space volume obtained from a single sample orientation. (b) Chemical structure of the compound. (c) Estimated number of peaks with a signal-to-noise ratio larger than three as a function of the counting time for a 0.001 mm$^3$ sample. (d) The simulated single-pulse peak of the [0 1 1] peak when a 0.125 mm$^3$ crystal is used. The peak is indicated within a circle in (a).

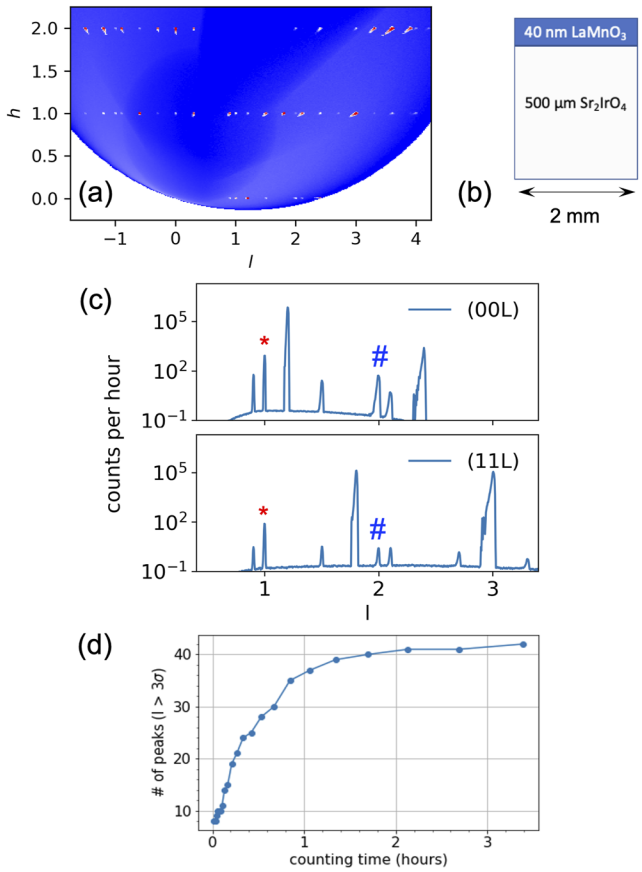


**FIG. 8.** Virtual experimental results from a 2 × 2 mm$^2$ epitaxial thin-film sample consisting of 40 nm $LaMnO_3$ grown on top of a 500 $\mu$m (001) $Sr_2IrO_4$ single-crystal substrate. (a) Scattering pattern taken at a single sample orientation in the *H0L* scattering plane, where the signal has been integrated over the full range of the *K* direction in the reciprocal space. (b) Nominal film structure. (c) Selected linecuts along the L direction. The ⋆ and # symbols label a few magnetic and nuclear film peaks, respectively. The other visible peaks are from the substrate. (d) Estimated number of film peaks with a single-to-noise ratio larger than three.

ratio ($I/\delta I$) larger than three within 5 min. There will be additional flux lost due to mirror misalignment and waviness, unavoidable background scattering, attenuation due to collimators, and imperfect detector performance for a real instrument, all of which will increase the required counting time. Additionally, it needs about ten orientations to obtain a complete dataset for structural refinements. Therefore, we estimate that for a 0.001 $mm^3$ crystal, the data collection rate will be about tens of minutes per frame and several hours per full dataset, making such experiments feasible. This unprecedented capability enables PIONEER to carry SCND experiments at the early stage of new materials discovery when large single crystals are often unavailable. It also offers the opportunity to use x-ray diamond anvil cells for high-pressure neutron experiments and use tiny crystals for accurate structural determination on high neutron-absorbing samples. At the same time, as shown in Fig. 7(d), the nuclear (0 1 1) peak acquires good counting statistics from a single-pulse exposure with a 0.125 $mm^3$ crystal. Therefore, PIONEER will be efficient for pulse-field experiments or time-resolved studies, even with sub-mm crystals.

The second case studies an epitaxial thin film on a home-grown single-crystal substrate, which often has a small surface area of a few square mm.[35] The sample is of a 2 × 2 $mm^2$ size, which consists of a 40 nm $LaMnO_3$ film grown on a 500 $\mu$m (001) $Sr_2IrO_4$ substrate. In this case, the scattering volume of interest is from the thin film, which is only $1.6 \times 10^{-4}$ $mm^3$. The volume ratio between the film and the substrate is 1: 12 500, and the incoherent scattering signal from the substrate is observable in Figs. 8(a) and 8(c), giving rise to a broad diffuse background. Nevertheless, good film signals can be obtained within one or two hours per frame, and the entire dataset takes less than a day to collect. We can further push the thickness limit down to 10 nm or less with a 5 × 5 $mm^2$ sample, the typical size for high-quality thin films grown using pulsed laser deposition (PLD) molecular-beam epitaxy (MBE) techniques. The results demonstrate that PIONEER can quantitatively study the nuclear and magnetic structures in ultra-thin films down to 10 nm or less thickness and potentially probe exotic surface or interface states.

## V. SUMMARY

In summary, PIONEER is a time-of-flight single-crystal diffractometer for tiny samples at the STS. It will cover a wide range of science cases, including quantum materials, energy and functional materials, and minerals. PIONEER has a high reciprocal-space resolution, enabling studies of crystals with chemically or magnetically modulated structures with long characteristic length scales up to 200 Å. PIONEER provides a high-flux polarized neutron beam, which will significantly enhance the sensitivity of the atomic magnetic susceptibility. The high beam brilliance, the low background, and the large detector array will enable PIONEER to study tiny crystals with volumes typical for x-ray diffraction experiments, i.e., 0.001 $mm^3$ or less, which is one-order-of magnitude smaller than the current limit. It also becomes feasible to study ultra-thin films of 10 nm thickness or less at PIONEER. With these novel capabilities, PIONEER will be a powerful tool to accelerate materials discovery to address energy, national security, and environmental challenges.

## ACKNOWLEDGMENTS

We sincerely thank the external science advisory board, Robert Birgeneau, Robert Cava, Martin Greven, Bo Iversen, Steven May, Ni Ni, Patrick Woodward, Stephen Wilson, Shan Wu, and Joe Zhou for identifying the scientific cases and defining the scientific requirements for PIONEER. We thank Koji Kaneko, Takashi Ohhara, and Ryoji Kiyanagi for discussion on SENJU at J- PARC; Werner Schweika and Fabrèges Xavier for discussion on MAGiC at ESS; Artur Glavic for discussion on ESTIA at ESS; Christina Hoffmann, Xiaoping Wang, and Feng Ye for discussion on TOPAZ and CORELLI at the SNS; and Bianca Haberl for discussion on DACs. This research used the resources of the Spallation Neutron Source Second Target Station Project at Oak Ridge National Laboratory (ORNL). ORNL is managed by UT-Battelle LLC for DOE's Office of Science, the single largest supporter of basic research in the physical sciences in the United States. The work at Argonne National Laboratory was supported by the U.S. Department of Energy, Office of Science, Basic Energy Sciences, Materials Sciences and Engineering Division.

## AUTHOR DECLARATIONS

### Conflict of Interest

The authors have no conflicts to disclose.

### Author Contributions

**Yaohua Liu:** Conceptualization (equal); Data curation (lead); Formal analysis (lead); Funding acquisition (equal); Investigation (lead); Methodology (lead); Project administration (equal); Validation (equal); Visualization (lead); Writing – original draft (lead); Writing – review & editing (lead). **Huibo Cao:** Conceptualization (equal); Funding acquisition (equal); Writing – review & editing (equal). **Stephan Rosenkranz:** Conceptualization (equal); Funding acquisition (equal); Writing – review & editing (equal). **Matthew Frost:** Conceptualization (supporting); Formal analysis (supporting); Funding acquisition (supporting); Investigation (supporting); Methodology (supporting); Writing – review & editing (equal). **Thomas Huegle:** Formal analysis (supporting); Investigation (supporting); Methodology (supporting); Writing – review & editing (equal). **Jiao Y. Y. Lin:** Formal analysis (supporting); Funding acquisition (supporting); Investigation (supporting); Methodology (supporting); Software (lead); Validation (equal). **Peter Torres:** Conceptualization (supporting); Funding acquisition (supporting); Investigation (supporting); Project administration (equal); Validation (supporting); Visualization (supporting). **Alexandru Stoica:** Conceptualization (supporting); Formal analysis (supporting); Funding acquisition (supporting); Methodology (supporting). **Bryan C. Chakoumakos:** Conceptualization (supporting); Funding acquisition (supporting); Writing – review & editing (equal).

## DATA AVAILABILITY

The data that support the findings of this study are available from the corresponding author upon reasonable request.

## REFERENCES


[1]J. C. Hemminger, J. Sarrao, G. Crabtree, G. Flemming, and M. Ratner, "Challenges at the frontiers of matter and energy: Transformative opportunities for discovery science," Technical Report No. OSTI/1283188, USDOE Office of Science (SC), 2015.

[2]C. Broholm, I. Fisher, J. Moore, M. Murnane, A. Moreo, J. Tranquada, D. Basov, J. Freericks, M. Aronson, A. MacDonald *et al.*, "Basic research needs workshop on quantum materials for energy relevant technology," Technical Report No. OSTI/1616509, USDOE Office of Science (SC), 2016.

[3]P. Adams, J. F. Ankner, L.-L. Anovitz, A. Banerjee, E. Begoli, R. Boehler, S. Calder, B. C. Chakoumakos, T. R. Charlton, W.-R. Chen *et al.*, "First experiments: New science opportunities at the Spallation Neutron Source Second Target Station (abridged)," Technical Report No. ORNL/SPR-2020/1437, Oak Ridge National Laboratory (ORNL), Oak Ridge, TN, 2020.

[4]A. J. Schultz, P. M. De Lurgio, J. P. Hammonds, D. J. Mikkelson, R. L. Mikkelson, M. E. Miller, I. Naday, P. F. Peterson, R. R. Porter, and T. G. Worlton, "The upgraded IPNS single crystal diffractometer," Physica B **385–386**, 1059–1061 (2006).

[5]D. A. Keen, M. J. Gutmann, and C. C. Wilson, "SXD—The single-crystal diffractometer at the ISIS Spallation Neutron Source," J. Appl. Crystallogr. **39**, 714–722 (2006).

[6]A. J. Schultz, M. R. V. Jørgensen, X. Wang, R. L. Mikkelson, D. J. Mikkelson, V. E. Lynch, P. F. Peterson, M. L. Green, and C. M. Hoffmann, "Integration of neutron time-of-flight single-crystal Bragg peaks in reciprocal space," J. Appl. Crystallogr. **47**, 915–921 (2014).

[7]T. Ohhara, R. Kiyanagi, K. Oikawa, K. Kaneko, T. Kawasaki, I. Tamura, A. Nakao, T. Hanashima, K. Munakata, T. Moyoshi *et al.*, "SENJU: A new time-of-flight single-crystal neutron diffractometer at J-PARC," J. Appl. Crystallogr. **49**, 120–127 (2016).

[8]K. H. Andersen, D. N. Argyriou, A. J. Jackson, J. Houston, P. F. Henry, P. P. Deen, R. Toft-Petersen, P. Beran, M. Strobl, T. Arnold *et al.*, "The instrument suite of the European Spallation Source," Nucl. Instrum. Methods Phys. Res., Sect. A **957**, 163402 (2020).

[9]See https://indico.esss.lu.se/event/723/attachments/5647/7744/magic_proposal_0.pdf for MAGiC proposal; accessed 31 May 2022.

[10]A. Gukasov and P. J. Brown, "Determination of atomic site susceptibility tensors from polarized neutron diffraction data," J. Phys.: Condens. Matter **14**, 8831 (2002).

[11]H. Cao, A. Gukasov, I. Mirebeau, P. Bonville, C. Decorse, and G. Dhalenne, "Ising versus *XY* anisotropy in frustrated $R_2Ti_2O_7$ compounds as 'Seen' by polarized neutrons," Phys. Rev. Lett. **103**, 056402 (2009).

[12]H. B. Cao, A. Gukasov, I. Mirebeau, and P. Bonville, "Anisotropic exchange in frustrated pyrochlore $Yb_2Ti_2O_7$," J. Phys.: Condens. Matter **21**, 492202 (2009).

[13]K. Ridier, B. Gillon, A. Gukasov, G. Chaboussant, A. Cousson, D. Luneau, A. Borta, J.-F. Jacquot, R. Checa, Y. Chiba *et al.*, "Polarized neutron diffraction as a tool for mapping molecular magnetic anisotropy: Local susceptibility tensors in $Co^{II}$ complexes," Chem. - Eur. J. **22**, 724–735 (2016).

[14]B. C. Chakoumakos and J. B. Parise, "Probing phase transitions and magnetism in minerals with neutrons," Elements **17**, 181–188 (2021).

[15]G. E. Ice, R. I. Barabash, and A. Khounsary, "Nested mirrors for X-rays and neutrons," Proc. SPIE **7448**, 74480B (2009).

[16]S. Weichselbaumer, G. Brandl, R. Georgii, J. Stahn, T. Panzner, and P. Böni, "Tailoring phase-space in neutron beam extraction," Nucl. Instrum. Methods Phys. Res., Sect. A **793**, 75–80 (2015).

[17]A. Glavic, J. Stahn, and S. Schütz, "Estia: Design of the polarized, small sample reflectometer at ESS," Swiss Neutron News **48**, 6–16 (2016), available at https://www.dora.lib4ri.ch/psi/islandora/object/psi:27312.

[18]P. Willendrup, E. Farhi, E. Knudsen, U. Filges, and K. Lefmann, "McStas: Past, present and future," J. Neutron Res. **17**, 35–43 (2014).

[19]P. Virtanen, R. Gommers, T. E. Oliphant, M. Haberland, T. Reddy, D. Cournapeau, E. Burovski, P. Peterson, W. Weckesser, J. Bright, S. J. van der Walt, M. Brett, J. Wilson, K. J. Millman, N. Mayorov, A. R. J. Nelson, E. Jones, R. Kern, E. Larson, C. J. Carey, I. Polat, Y. Feng, E. W. Moore, J. VanderPlas, D. Laxalde, J. Perktold, R. Cimrman, I. Henriksen, E. A. Quintero, C. R. Harris, A. M. Archibald, A. H. Ribeiro, F. Pedregosa, P. van Mulbregt, and SciPy 1.0 Contributors, "SciPy 1.0: Fundamental algorithms for scientific computing in Python," Nat. Methods **17**, 261–272 (2020).

[20]C. Schanzer, M. Schneider, and P. Böni, "Neutron optics: Towards applications for hot neutrons," J. Phys.: Conf. Ser. **746**, 012024 (2016).

[21]K. H. Andersen, M. Bertelsen, L. Zanini, E. B. Klinkby, T. Schönfeldt, P. M. Bentley, and J. Saroun, "Optimization of moderators and beam extraction at the ESS," J. Appl. Crystallogr. **51**, 264–281 (2018).

[22]C. Zendler and P. M. Bentley, "Systematic neutron guide misalignment for an accelerator-driven spallation neutron source," Phys. Rev. Accel. Beams **19**, 083501 (2016).

[23]U. B. Hansen, M. Bertelsen, E. B. Knudsen, and K. Lefmann, "Simulation of waviness in neutron guides," J. Neutron Res. **18**, 45–59 (2015).

[24]R. A. Riedel, C. Donahue, T. Visscher, and C. Montcalm, "Design and performance of a large area neutron sensitive anger camera," Nucl. Instrum. Methods Phys. Res., Sect. A **794**, 224–233 (2015).

[25]M. B. Stone, J. L. Niedziela, M. A. Overbay, and D. L. Abernathy, "The ARCS radial collimator," EPJ Web Conf. **83**, 03014 (2015).

[26]F. Islam, J. Lin, T. Huegle, I. Lumsden, D. Anderson, A. Elliott, B. Haberl, and G. Granroth, "Computational optimization of a 3D printed collimator," J. Neutron Res. **22**, 155–168 (2020).

[27]See https://neutrons.ornl.gov/topaz for TOPAZ at SNS; accessed 31 May 2022.

[28]E. O. Lazo, S. Antonelli, J. Aishima, H. J. Bernstein, D. Bhogadi, M. R. Fuchs, N. Guichard, S. McSweeney, S. Myers, K. Qian *et al.*, "Robotic sample changers for macromolecular X-ray crystallography and biological small-angle X-ray scattering at the National Synchrotron Light Source II," J. Synchrotron Radiat. **28**, 1649 (2021).

[29]G. E. Granroth, K. An, H. L. Smith, P. Whitfield, J. C. Neuefeind, J. Lee, W. Zhou, V. N. Sedov, P. F. Peterson, A. Parizzi *et al.*, "Event-based processing of neutron scattering data at the Spallation Neutron Source," J. Appl. Crystallogr. **51**, 616–629 (2018).

[30]B. Haberl, S. Dissanayake, Y. Wu, D. A. A. Myles, A. M. Dos Santos, M. Loguillo, G. M. Rucker, D. P. Armitage, M. Cochran, K. M. Andrews *et al.*, "Next-generation diamond cell and applications to single-crystal neutron diffraction," Rev. Sci. Instrum. **89**, 092902 (2018).

[31]See https://neutrons.ornl.gov/sample for Sample Environments at SNS and HFIR; accessed 31 May 2022.

[32]J. Y. Y. Lin, H. L. Smith, G. E. Granroth, D. L. Abernathy, M. D. Lumsden, B. Winn, A. A. Aczel, M. Aivazis, and B. Fultz, "MCViNE—An object oriented Monte Carlo neutron ray tracing simulation package," Nucl. Instrum. Methods Phys. Res., Sect. A **810**, 86–99 (2016).

[33]J. Y. Y. Lin, F. Islam, G. Sala, I. Lumsden, H. Smith, M. Doucet, M. B. Stone, D. L. Abernathy, G. Ehlers, J. F. Ankner *et al.*, "Recent developments of MCViNE and its applications at SNS," J. Phys. Commun. **3**, 085005 (2019).

[34]K. H. Lii, C. C. Wang, R. K. Chiang, and S. L. Wang, "The structure of $CsV(MoO_4)_2$," J. Solid State Chem. **80**, 144–148 (1989).

[35]E. J. Moon, A. F. May, P. Shafer, E. Arenholz, and S. J. May, "Growth and electrical transport properties of $La_{0.7}Sr_{0.3}MnO_3$ thin films on $Sr_2IrO_4$ single crystals," Phys. Rev. B **95**, 155135 (2017).